

Two different incorporation routes of cellulose nanocrystals in waterborne polyurethane nanocomposites (<http://dx.doi.org/10.1016/j.eurpolymj.2016.01.035>)

*Arantzazu Santamaria-Echart, Lorena Ugarte, Aitor Arbelaiz, Nagore Gabilondo, Maria Angeles Corcuera, Arantxa Eceiza*

Group 'Materials + Technologies', Department of Chemical and Environmental Engineering, Polytechnic School, University of the Basque Country, Pza Europa 1, Donostia-San Sebastian 20018, Spain

## ABSTRACT

The renewability, availability and low-cost of eco-friendly cellulose nanocrystals (CNC), have gaining attention for nanocomposites preparation due to their unique properties in the nanoscale and their water dispersibility, becoming a suitable reinforcement in water-borne polyurethane (WBPU) dispersions. Thereby, a WBPU matrix with a high hard segment content (about 48 wt%) was synthesized resulting in a dispersion of low particle size with a narrow distribution analyzed by means of dynamic light scattering and visually stable over 6 months. The CNC reinforcement isolated from microcrystalline cellulose via acid hydrolysis lead to CNC with a high length/diameter aspect ratio of about 31, determined by atomic force microscopy. In the nanocomposites preparation, two incorporation routes were designed for analyzing the influence of CNC disposition in the nanocomposites films: the classical mixing by sonication or in-situ adding CNC in water during particles formation step. The influence of CNC addition route and their disposition in the final properties of nanocomposites were analyzed by Fourier transform infrared spectroscopy, differential scanning calorimetry, thermogravimetric analysis, dynamic mechanical analysis, atomic force microscopy and dynamic water contact angle, observing considerable variations by adding 1 and 3 wt% of CNC. The reinforcement addition route influenced the WBPU-CNC interactions, which resulted more effective by the alternative in-situ incorporation method. The CNC incorporation restricted the crystallization of soft domains, in a higher extend in nanocomposites prepared by in-situ route, and improved the thermomechanical stability. The studied CNC incorporation routes lead to different dispositions of CNC in the matrix, resulting in different mechanical performance, providing a suitable stress transfer in the nanocomposite and diverse hydrophilic behavior, comparing with the WBPU matrix.

## 1. Introduction

Segmented polyurethanes are block copolymers with alternating hard and soft segments that separate in microphases due to the incompatibility between both segments [1]. The hard segment (HS) provides usually the rigidity and strength to the polymer whereas the soft segment (SS) confers flexibility. Thereby, considering the variety in the chemical constituents and composition, it is possible to synthesize specific polyurethanes with particular properties [2], opening a wide range of application fields. Conventional polyurethanes are solventborne systems, but the environmental awareness has promoted the development of waterborne polyurethane (WBPU) systems by the addition of internal emulsifiers [3], avoiding the use of organic solvents and obtaining stable water dispersions over months. With the purpose of synthesizing new environmentally friendly materials, WBPU has been employed in the preparation of nanocomposites. The chance to disperse hydrophilic reinforcement in WBPU, has focused attention in water dispersible entities, such as cellulose derivatives. Cellulose is the most abundant renewable biopolymer which has attracted great attention due to the availability, low cost, non-toxicity, biocompatibility

and biodegradability. Cellulose is produced principally in nature by plants like cotton, jute or flax, different marine animals as tunicates, and in invertebrates, fungi, algae, bacteria, and amoeba (protozoa) in lower quantities [4,5]. Cellulose can be used in different dimensions, from macroscopic to nanoscale, and diverse assemblies such as fibers or crystals [6]. Among these, it is worth noting the relevance of cellulose nanocrystals (CNC) which are gaining importance in diverse application fields [4,7]. The isolation of the crystalline ordered regions of cellulose lead to obtaining those highly crystalline nanoentities, possessing unique properties in the nanoscale dimension, modulated by isolation hydrolysis process [8] and origin of cellulose [5]. The high length/diameter aspect ratio and high specific mechanical properties are focusing the attention of CNC in nanocomposites field [9]. Several strategies have been used in order to prepare cellulose well dispersed nanocomposites, such as melt blending or solvent casting. In the former case, it is difficult to obtain the adequate cellulose dispersion in the matrix and high temperatures could degrade nanocellulose nanocrystals [10]. By solvent-casting, the slow evaporation of the solvent promotes the formation of hydrogen bonds and rigid networks, resulting in high thermomechanical stability and mechanical reinforcement in the nanocomposites. Diverse types of polymers have been used for nanocellulose nanocomposites preparation [11]. The use of nonpolar polymers requires an appropriate organic dispersion medium or the use of surfactant or surface chemical modification of nanocellulose in order to obtain a suitable polymer matrix dispersion. Instead, the use of aqueous polymer dispersions ensures the compatibility between the polymer and nanocellulose in water, facilitating the good dispersion for homogeneous nanocomposites preparation without requiring chemical modifications or surfactants [10]. The chance to disperse hydrophilic CNC in WBPU, has focused their attention in WBPU–CNC nanocomposites. There are different works analyzing the final properties of CNC reinforced WBPU [12], but few works consider CNC addition strategy and its effect in the final disposition of CNC in the matrix. Thereby, in this work the synthesis of WBPU dispersion and the isolation of CNC have been carried out for the preparation of nanocomposites considering CNC addition protocol. Therefore, two CNC incorporation routes were designed for the analysis of CNC arrangement in the WBPU matrix: the classical mixing by sonication after WBPU synthesis and the alternative in-situ during the WBPU synthesis process. The effect of CNC addition as well as the incorporation procedure has been analyzed in the final properties of the nanocomposites.

## **2. Experimental**

### **2.1. Materials**

CNC were isolated from microcrystalline cellulose (MCC) powder supplied from Aldrich and sulfuric acid ( $\text{H}_2\text{SO}_4$ ) (96%) was provided from Panreac. For WBPU synthesis, poly( $\epsilon$ -caprolactone) diol (PCL) ( $\overline{M}_w = 2000 \text{ g mol}^{-1}$ ), purchased from BASF was chosen as soft segment and 1,4 butanediol (BD), supplied from Aldrich as chain extender, being dried in a rotary evaporator at 50 °C for 4 h. Isophorone diisocyanate (IPDI) was kindly supplied from Bayer, and dibutyl tin dilaurate (DBTDL) was purchased from Aldrich. 2,2-Bis(hydroxymethyl)propionic acid (DMPA) purchased from Aldrich and used as internal emulsifier, was dried at 55 °C for 4 h under vacuum. Hydranal-molecular Sieve 0.3 nm (water adsorption capacity of 15%), supplied by Fluka, and previously dried at 55 °C under vacuum for 1 day was employed for dehydration of triethylamine (TEA), both provided from Aldrich. N,N-dimethylformamide (DMF) and tetrahydrofuran (THF), were also provided by Aldrich.

## **2.2. Isolation of cellulose nanocrystals**

CNC were isolated from microcrystalline cellulose via sulfuric acid hydrolysis removing the amorphous regions of cellulose. The isolation was carried out following previously reported method [13]. Briefly described, MCC were mixed with H<sub>2</sub>SO<sub>4</sub> (64 wt%) at 45 °C for 30 min. The suspension was diluted with deionized water and after washed by centrifugation, the suspension was subjected to a dialysis process against deionized water until pH remained constant around 5–6. Thus, CNC dispersion with about 0.5 wt% concentration was obtained.

## **2.3. Synthesis of waterborne polyurethane**

WBPU with a HS content of about 48 wt% was synthesized by two step polymerization process with the PCL:IPDI:DMPA: BD molar composition of 0.5:3.15:0.5:2 considering PCL as SS and IPDI, DMPA and BD as HS. According to previously published protocol [14], the reaction was carried out in a 250 mL four-necked flask placed in a thermostated bath and equipped with a mechanical stirrer, thermometer, condenser and nitrogen inlet. The progress of each reaction step was determined by dibutylamine back titration according to ASTM D 2572-97. In the first step PCL and IPDI were reacted with 0.1 wt% of DBTDL at 90 °C. Then, DMPA was added and allowed to react until the theoretical NCO content was reached. In the second step BD was added for the chain extension. Thereafter, the necessary amount of TEA was added in order to neutralize DMPA carboxylic groups and the polymer was cooled to room temperature while the viscosity was adjusted with THF. Finally, deionized water was added dropwise under vigorous stirring and THF was removed using a rotary evaporator, obtaining a dispersion with a solid content of about 25 wt%.

## **2.4. Nanocomposites preparation**

Polyurethane nanocomposites reinforced with 1 and 3 wt% CNC were prepared by two CNC incorporation routes; mixing WBPU and CNC by sonication and in-situ during WBPU synthesis. In the first case, CNC dispersion was sonicated for 1 h and after the addition of the WBPU dispersion, the mixture was sonicated for another 1 h. In the second case, previously sonicated CNC dispersion was incorporated to the polyurethane in the water addition step of the synthesis. Both dispersions were cast in Teflon molds allowing to dry in a climatic chamber at 25 °C and 50% of relative humidity during 7 days and finally in a vacuum oven. Furthermore, neat polyurethane dispersion matrix was cast following the conditions used for nanocomposites films preparation. Designation of obtained films is expressed as WBPU in the case of the matrix and WBPU-Xson and WBPU-Xsyn for the nanocomposites prepared mixing by sonication and in-situ respectively, where X denotes CNC weight content in the nanocomposite. The WBPU and nanocomposites were stored in a desiccator for 1 week before their characterization.

## **2.5. Characterization**

### **2.5.1. Dynamic light scattering**

WBPU and in-situ synthesized nanocomposites dispersion particle size and distribution was determined by dynamic light scattering (DLS) using a BI-200SM goniometer from Brookhaven. The intensity of dispersed light was measured at 90° using a luminous source of He-Ne laser (Mini L-30, wavelength  $\lambda = 637$  nm, 400 mW) and a detector (BI-APD) placed on a rotary arm. Samples prepared by mixing a small amount of aqueous dispersion with ultrapure water were analyzed at 25 °C by triplicate.

### 2.5.2. Sulfate groups concentration anchored to CNC

The concentration of sulfate groups anchored to the sulfuric acid hydrolyzed cellulose nanocrystals was determined by conductometric titration at 25 °C with a Crison EC-Meter GLP 31 conductometer calibrated with 147  $\mu\text{S cm}^{-1}$ , 1413  $\mu\text{S cm}^{-1}$  and 12.88  $\text{mS cm}^{-1}$  standards. For the titration, NaOH and HCl 10 mM were used. Sulfate groups concentration was also determined by elemental analysis in a Euro EA3000 Elemental Analyzer of Eurovector.

### 2.5.3. Fourier transform infrared spectroscopy

WBPU, CNC and nanocomposites characteristic functional groups were analyzed by Fourier transform infrared spectroscopy (FTIR) using a Nicolet Nexus spectrometer provided with a MKII Golden Gate accessory (Specac) with diamond crystal at a nominal incidence angle of 45° and ZnSe lens. Measurements were run averaging 64 scans with a resolution of 8  $\text{cm}^{-1}$  in the range between 4000 and 650  $\text{cm}^{-1}$ .

### 2.5.4. Differential scanning calorimetry

The thermal properties of WBPU and nanocomposites were determined by differential scanning calorimetry (DSC) in a Mettler Toledo 822e equipment provided with a robotic arm and an electric intracooler as refrigerator unit. Between 5 and 10 mg of samples were encapsulated in aluminum pans and heated from 75 to 180 °C at a scanning rate of 20 °C  $\text{min}^{-1}$  in nitrogen atmosphere. The glass transition temperature was fixed as the inflection point of the heat capacity change. The maximum of endothermic peak was settled as the melting temperature considering the area under the peak as melting enthalpy.

### 2.5.5. Thermogravimetric analysis

The thermal stability of CNC and WBPU and nanocomposites films was determined by thermogravimetric analysis (TGA) using a TGA/SDTA 851 Mettler Toledo. Between 5 and 10 mg of samples were subjected to a dynamic run from 25 to 700 °C at a heating rate of 10 °C  $\text{min}^{-1}$  in nitrogen atmosphere. The initial degradation temperature was referred to the loss of 5 wt% of the total sample decomposition whereas the maximum degradation temperature was settled as the minimum of the degradation peak in the derivative thermogravimetric (DTG) curves.

### 2.5.6. Mechanical testing

Mechanical behavior of films were determined at room temperature using a MTS Insight 10 testing machine provided with a 250 N load cell and pneumatic grips to hold samples. Films tensile modulus, yield stress, stress at break and strain at break were determined from stress–strain curves performed at a crosshead speed of 50  $\text{mm min}^{-1}$ . Five specimens of 8 mm in length, 2.5 mm in width and 0.4 mm in thickness were analyzed for each system.

### 2.5.7 Dynamic mechanical analysis

The thermomechanical stability of the films was determined by dynamic mechanical analysis (DMA) using an Eplexor 100 N analyser Gabo equipment. The measurements carried out in tensile mode were performed from 100 to 150 °C at a scanning rate of 2 °C  $\text{min}^{-1}$ . The initial strain was established as 0.05% and the operating frequency was fixed at 1 Hz.

### 2.5.8 Atomic force microscopy

The morphology of CNC and WBPU and their nanocomposites was determined by atomic force microscopy (AFM). The images were obtained at room temperature in tapping mode, using a Nanoscope IIIa scanning probe microscope (Multimode™ Digital instruments) with an integrated force generated by cantilever/silicon probes, applying a resonance frequency of about 180 kHz. The cantilever had a tip radius of 5–10 nm and was 125 μm long. Samples were prepared via spin-coating (Spincoater P6700) at 200 rpm for 130 s. WBPU and nanocomposites samples were prepared by spin-coating a droplet of the dispersion on glass supports whereas a droplet of CNC diluted dispersion was spin-coated on a mica flake.

### 2.5.9 Dynamic water contact angle

The hydrophilicity of WBPU and nanocomposites films was determined by dynamic water contact angle (DWCA) using a Dataphysics OCA20 equipment at room temperature. Four measurements of each sample were performed by sessile drop method. Deionized water 3 μL drop was deposited in the surface of the film by a syringe tip. The needle was remained inside the drop, maintaining the smallest portion as possible during all experiment, in order to prevent alterations in the tests. The advancing contact angle values were measured by increasing the drop volume adding deionized water at a constant flow of 0.5 μL, while receding contact angles were determined reducing the drop volume.

## 3. Results and discussion

### 3.1. Cellulose nanocrystals characterization

AFM images observed in Fig. 1 corroborate the isolation of CNC nanoentities via acid hydrolysis showing a rod-like morphology. In order to determine the length/diameter (L/D) aspect ratio, around 100 CNCs were measured and averaged. The length of CNCs was determined in the height image, Fig. 1a, whereas the diameters were measured in the AFM height profiles, Fig. 1c, assuming their cylindrical shape [15]. Thereby, CNCs with an average diameter of  $5.4 \pm 1.5$  nm and length about  $167 \pm 31$  nm were obtained, corresponding to an L/D aspect ratio of about 31.

The CNC isolation by sulfuric acid hydrolysis process introduces sulfate groups in the CNCs surface providing stability in aqueous suspension due to electrostatic repulsion interactions [8,16]. In this case, the CNCs exhibit a sulfur content of 1.22% measured by conductometric titration [8,17]. Elemental analysis was also performed obtaining a similar sulfur content of 1.28%. This values support the modification of negatively charged CNCs surface as a result of the hydrolysis.

### 3.2. Nanocomposites characterization

Particle size and polydispersity of WBPU matrix and in-situ synthesized WBPU-1<sub>syn</sub> nanocomposite dispersions are summarized in Table 1. It can be observed that small particles with a narrow distribution were obtained, leading to visually stable dispersions over 6 months. Moreover, the addition of 1 wt% of CNC in-situ during the water addition process, does not affect the formation of the particles. Despite the higher length of CNC, similar particle size and polydispersity were measured in both cases. Instead, in the case of WBPU-3<sub>syn</sub>, it was not possible to determine the particle size since the higher CNC content interferes in its determination.

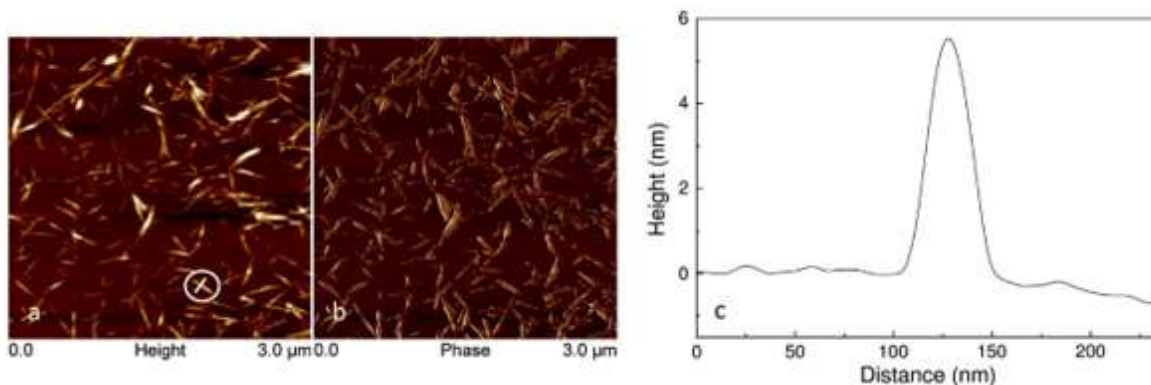


Fig. 1. AFM height (a) and phase (b) images of cellulose nanocrystals. (c) Height profile of cellulose nanocrystal indicated in height image.

Table 1. Particle size and polydispersity of dispersions

Sample	Diameter (nm)	Polydispersity
WBPU	$52.3 \pm 0.5$	$0.08 \pm 0.05$
WBPU-1 <sub>syn</sub>	$52.6 \pm 0.2$	$0.06 \pm 0.02$

The WBPU and 1 wt% CNC reinforced nanocomposites films prepared from the dispersions by means of the two different CNC incorporation routes are shown in Fig. 2. Although only WBPU and nanocomposites containing 1 wt% are shown in Fig. 2, nanocomposites containing 3 wt% of CNC resulted also transparent. In addition, all samples were completely soluble in THF and DMF.



Fig. 2. (a) WBPU matrix, (b) WBPU-1<sub>son</sub> and (c) WBPU-1<sub>syn</sub> nanocomposites films prepared by casting.

The structure and hydrogen bonding interactions between CNC and WBPU were studied by FTIR. Fig. 3 shows spectra of nanocomposites and neat components. Two typical regions have been analyzed. In the interval from  $3600$  to  $3100$   $\text{cm}^{-1}$  neat WBPU shows the stretching vibration related to N-H of urethane groups and CNC shows a broad band related with OH stretching vibration [18]. Slight differences can be observed between the nanocomposites and neat WBPU. The peak observed about  $3340$   $\text{cm}^{-1}$  is related with the N-H vibration of urethane groups associated by hydrogen bonding interactions. In WBPU-1<sub>son</sub> and WBPU-3<sub>son</sub> samples, an extended shoulder around  $3530$   $\text{cm}^{-1}$ , similar to the observed in CNC spectrum

can be appreciated whereas in WBPU-1<sub>syn</sub> and WBPU-3<sub>syn</sub> is barely noticeable. It could be related with the CNC disposition in the nanocomposite. In the case of mixing components by sonication, CNC are homogeneously dispersed in WBPU and OH groups of CNC are also appreciable by broadening the peak in that region to higher wavenumbers, similar to the peak observed in CNC spectrum. However, in-situ incorporation route favors the intercalation of CNC in WBPU particles during dispersion formation, and considering ATR-FTIR as surface physicochemical analysis, it is thought that CNC could result embedded in the matrix during film formation, hindering the visualization of CNC hydroxyl groups, but favoring interactions between them. Regarding to the carbonyl region, an amplification of the spectra has been included in Fig. 3b. The broadening and increase of the relative intensity of the peak related with the hydrogen bonded C=O around 1700 cm<sup>-1</sup> respect to the free C=O groups about 1720 cm<sup>-1</sup>, suggests the existence of WBPU–CNC interactions in the nanocomposites, which increases with CNC content.

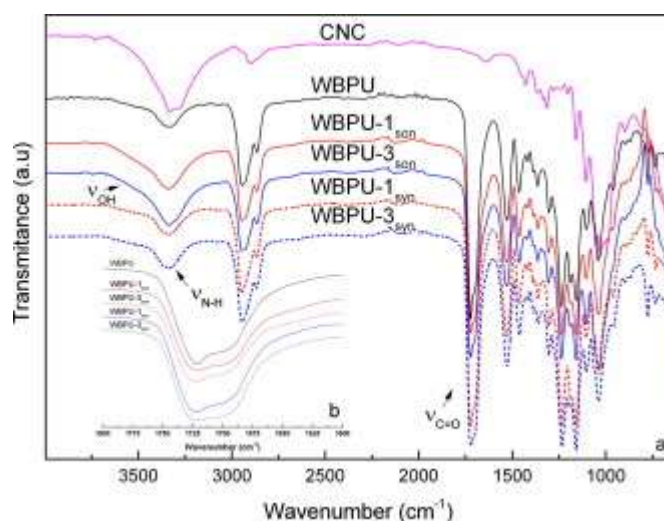


Fig. 3. (a) FTIR spectra of the matrix and the nanocomposites and (b) an amplification of the carbonyl stretching region.

Thermal behavior of the films was studied by DSC. The thermograms are displayed in Fig. 4. The thermal transition values corresponding to the soft domain glass transition temperature ( $T_{gSS}$ ), melting temperature ( $T_{mSS}$ ) and enthalpy ( $\Delta H_{mSS}$ ) obtained from the curves are summarized in Table 2. Analyzing soft domain melting endothermic peak, it has been observed that the addition of CNC decreases the melting enthalpy of the nanocomposites. The WBPU-CNC interactions presumably restrict soft segment chains to arrange in crystalline domains [19], providing higher mobility to soft segment chains [20,21] and hence, observing a slight decrease in  $T_{gSS}$  values. Furthermore, the lower  $T_{mSS}$  and  $\Delta H_{mSS}$  values in WBPU-1<sub>syn</sub> comparing with WBPU-1<sub>son</sub>, suggests the greater WBPU-CNC interactions, which would hinder in a greater extent crystals growth. Indeed, at higher CNC content, for WBPU-3<sub>syn</sub>, soft domain crystallization is totally hindered. In this case, WBPU-CNC interactions lead to a clearer broad transition around 85 °C related with the short range order of hard segment [22], which restricts soft segment chains mobility and increases slightly  $T_{gSS}$ .

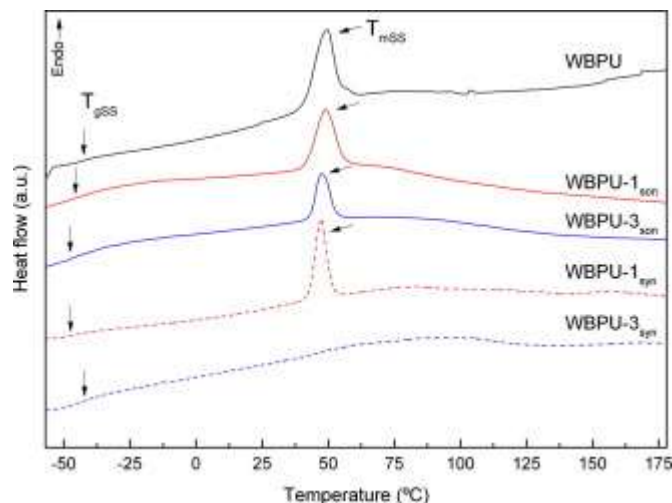


Fig. 4. DSC thermograms of WBPU matrix and the nanocomposites

Table 2. Thermal properties of the films

Sample	$T_{gSS}$ (°C)	$T_{mSS}$ (°C)	$\Delta H_{mSS}$ (J g <sup>-1</sup> )
WBPU	-42.7	49.5	10.8
WBPU-1 <sub>son</sub>	-45.8	49.1	7.1
WBPU-3 <sub>son</sub>	-47.5	47.5	4.1
WBPU-1 <sub>syn</sub>	-47.3	47.2	6.0
WBPU-3 <sub>syn</sub>	-42.0	-	-

The thermal stability of CNC and WBPU and nanocomposites films analyzed by TGA curves are exhibited in Fig. 5a and DTG curves, where the rate of weight loss can be analyzed, are displayed in Fig. 5b. In polyurethanes, a unique degradation stage as well as multiple degradation stages have been observed, influenced by the polyurethane nature, composition, crystallinity and microphase separation degree of the system, among others [23–25]. In this case, the neat WBPU shows a single decomposition peak with the maximum degradation temperature centered at 331 °C, whereas in nanocomposites a shoulder can also be observed. The initial degradation temperature ( $T_i$ ), the maximum degradation temperature ( $T_m$ ) and the temperature of the shoulder observed in nanocomposites ( $T_s$ ) are summarized in Table 3. It has been observed an increase in the  $T_i$  and  $T_m$  values in the nanocomposites comparing with the matrix, attributable to the stabilization of urethane groups by interactions of WBPU and CNC and the enhancement of the thermal resistance with CNC addition. Analyzing  $T_i$  and  $T_m$  values, the CNC addition by sonication and in-situ causes a delay of 5–7 °C in the start of the degradation process and a delay around 30 °C in the  $T_m$  values. This remarkable improvement, could be owed to a suitable dispersion of the CNC in the WBPU matrix [21,26] providing interactions. Analyzing CNC degradation curves, multiple decomposition steps can be observed related with sulfate groups [27,28], where the maximum degradation temperatures are centered at 239 and 325 °C. Otherwise, the shoulder observed around 315–320 °C in the degradation of the nanocomposites could be attributed to the less ordered domains induced by the interactions between WBPU and CNC in the polyurethane.

Table 3. Initial degradation, maximum degradation and shoulder temperatures of the WBPU matrix and nanocomposites.

Sample	$T_i$ (°C)	$T_m$ (°C)	$T_s$ (°C)
WBPU	281	331	–
WBPU-1 <sub>son</sub>	288	359	322
WBPU-3 <sub>son</sub>	287	365	316
WBPU-1 <sub>syn</sub>	286	362	323
WBPU-3 <sub>syn</sub>	288	361	313

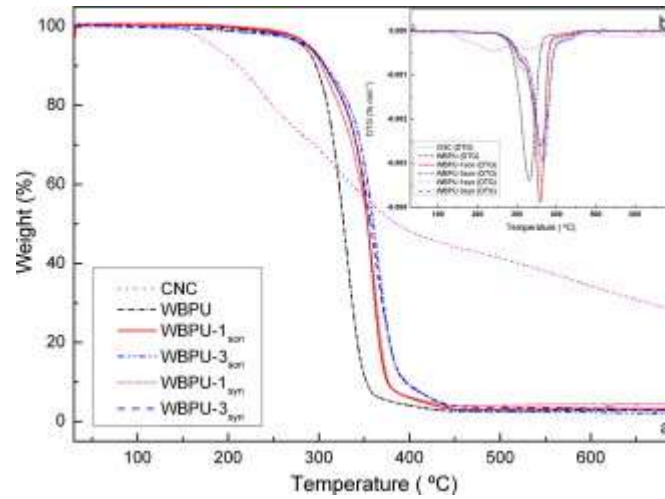


Fig. 5. (a) TGA and (b) DTG curves of CNC, WBPU matrix and nanocomposites.

Fig. 6 shows stress–strain curves of the films. Modulus, stress at yield, stress at break and strain at break values determined from the curves are summarized in Table 4. It can be observed that mechanical properties depend on both, CNC content as well as CNC addition route. In the case of CNC addition by sonication, where WBPU soft segments order in crystalline domains, higher modulus and stress at yield values and lower strain at break values are obtained as CNC content is increased [29]. In the case of in-situ method and at 1 wt% of CNC, an increase in modulus and stress at yield values and a decrease in strain at break value are also observed comparing with the matrix. However, at 3 wt% of CNC, modulus and stress at yield decrease, attributable to the absence of soft ordered domains, as observed by DSC results. In turn, stress at break and strain at break values increase respect to 1 wt% of CNC owing to the additional resistance provided by CNC and chain mobility. These improvements suggest the effective reinforcement effect caused by CNCs due to new interactions with the WBPU, maintaining a suitable stress transfer in the nanocomposite besides their morphology with an elevated L/D aspect ratio [30]. By this way, tailored mechanical properties can be obtained attending to the CNC addition method as well as content. When CNC are added by sonication, the strain induced crystallization of the matrix is maintained. Nevertheless, when CNCs are added during the synthesis process, the system results in sharper WBPU-CNC interactions, hindering the orientation and crystallization of the WBPU under strain [13]. Otherwise, the possible reaction of residual isocyanate groups (isocyanate/ hydroxyl groups ratio of 1.05) with hydroxyl groups of CNC

could only occur by in-situ method during water/CNC addition step, which could contribute to enhance the interactions between them [31].

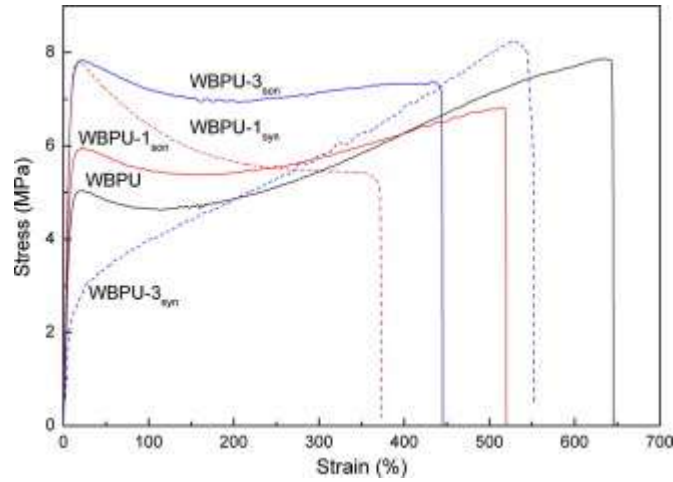


Fig. 6. Stress vs. strain curves of WBPU matrix and nanocomposites

Table 4. Mechanical properties of the films.

Sample	Modulus (MPa)	Stress at yield (MPa)	Stress at break (MPa)	Strain at break (%)
WBPU	54.8 ± 5.7	4.6 ± 0.3	7.9 ± 0.4	735 ± 102
WBPU-1 <sub>son</sub>	79.0 ± 0.9	5.7 ± 0.8	6.4 ± 0.5	472 ± 29
WBPU-3 <sub>son</sub>	88.1 ± 2.5	8.3 ± 0.7	7.4 ± 0.6	391 ± 58
WBPU-1 <sub>syn</sub>	88.2 ± 5.9	7.8 ± 0.3	5.5 ± 0.2	374 ± 79
WBPU-3 <sub>syn</sub>	31.9 ± 3.3	3.2 ± 0.1	8.4 ± 0.6	533 ± 30

The thermomechanical stability of the films was analyzed by monitoring the evolution of storage modulus ( $E'$ ) and  $\text{Tan}\delta$  curves as a function of temperature, which are shown in Fig. 7. At low temperatures, in the glassy state, it can be observed that nanocomposites show higher  $E'$  values comparing with the matrix, which increase with CNC addition, due to the effective CNC reinforcement [32] and soft segment ordered structures. In the case of WBPU-3<sub>syn</sub>, the absence of soft segment crystallization results in similar  $E'$  values to WBPU-1<sub>syn</sub>. In the range between -50 and -30 °C, a pronounced decrease is observed owing to a glassy relaxation. This change in  $E'$  curves, generally reflected by a peak in  $\text{Tan}\delta$  curves, is related with the  $T_{g_{SS}}$  of the films. Once amorphous WBPU chains acquire mobility, as temperatures increases, a progressive decrease is observed in  $E'$ , resulting sharper next to soft segment crystalline domains melting transition. Afterward, an abrupt drop is observed (between 30 and 50 °C) in agreement with DSC results. In the case of WBPU-3<sub>syn</sub>, though  $E'$  values remain always above the matrix due to the reinforcement provided by the CNC, the absence of soft ordered domains leads to the earlier  $E'$  drop as  $T_{g_{SS}}$  is exceeded. Moreover, the effective CNC dispersion in the nanocomposites provides an improvement of about 20-30 °C in the thermomechanical stability of nanocomposites.

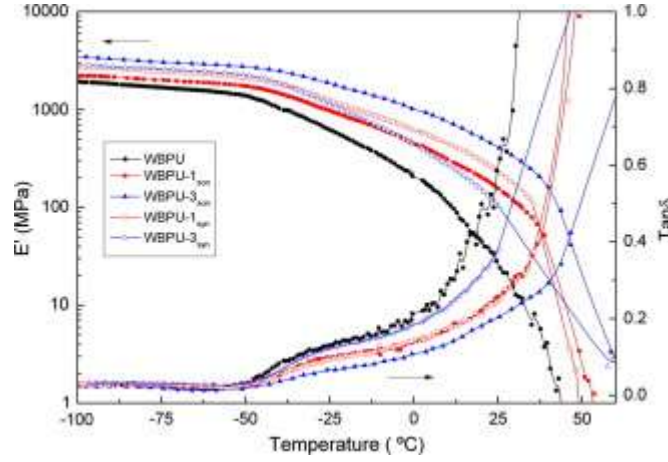


Fig. 7. Storage modulus and Tan $\delta$  curves of WBPU matrix and nanocomposites.

Regarding to the CNC reinforcement effect, it is possible to estimate the physical crosslinking density ( $v_s/V$ ) of the WBPU matrix and the nanocomposites analyzing the  $E'$  in the rubbery plateau by the equations [33]:

$$(v_s/V) = A \exp(E_a/RT) \quad (1)$$

$$E' = (v_s/V)RT = ART \exp(E_a/RT) \quad (2)$$

Eq. (2), can be also expressed by:

$$\ln(E'/T) = \ln RA + E_a/RT \quad (3)$$

where  $A$  is a constant,  $E_a$  is the apparent activation energy of hydrogen bonding dissociation,  $R$  is the gas constant and  $T$  is the absolute temperature. Thereby, plotting  $\ln E'/T$  versus  $1/T$ , it is possible to determine  $E_a$  and  $A$  values from Eq. (3). In this case, considering curves as straight lines,  $E_a$  values of 28.7, 20.2, 16.9, 18.3 and 25.1  $\text{kJ mol}^{-1}$  and  $A$  values of  $2.9 \cdot 10^{-7}$ ,  $2.7 \cdot 10^{-5}$ ,  $2.6 \cdot 10^{-4}$ ,  $8.8 \cdot 10^{-5}$  and  $3.1 \cdot 10^{-6} \text{ mol m}^{-3}$  were determined for WBPU, WBPU-1<sub>son</sub>, WBPU-3<sub>son</sub>, WBPU-1<sub>syn</sub> and WBPU-3<sub>syn</sub> respectively. As a result, ( $v_s/V$ ) can be quantified in function of temperature from Eq. (1) as it is displayed in Fig. 8. As it was expected, and in accordance with mechanical test results, the physical crosslinking density increases considerably with the addition of CNC, except for WBPU-3<sub>syn</sub> once  $T_{gSS}$  is exceeded. In addition, it can be appreciated a drop in ( $v_s/V$ ) regarding to the crosslinking disruption as temperature increases, which is retarded with CNCs addition, once again except for WBPU-3<sub>syn</sub>. It could be attributed to the different structure adopted by the polyurethane in the WBPU-3<sub>syn</sub> as observed in DSC results.

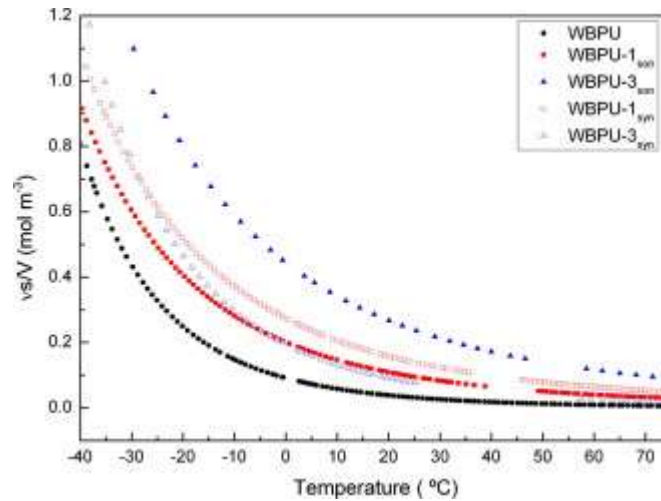


Fig. 8. Physical crosslinking density of films

Fig. 9 shows AFM height and phase images of WBPU matrix and height images of nanocomposites with 1 wt% of CNC. In all images, WBPU light and dark regions are appreciated associated with the crystalline and amorphous domains, respectively. Analyzing nanocomposites, it can be observed a homogeneous distribution of CNC in the WBPU, without the presence of agglomerates implying the proper dispersion of the reinforcement in the matrix and the formation of WBPU-CNC interactions during film forming by casting. However, some differences can be distinguished comparing both nanocomposite images. In the case of WBPU-1<sub>son</sub>, CNC in all of its length and dispersed homogeneously in the matrix are observed. In sample WBPU-1<sub>syn</sub> instead, CNC seem to be shorter despite possessing the same aspect ratio. So, this fact would imply that CNC are partially embedded in the matrix due to the greater intercalation among WBPU particles when were added during such particles formation. Thereby, the diverse arrangement adopted by CNCs in the nanocomposites, justify the variation in the physicochemical and mechanical properties of the films.

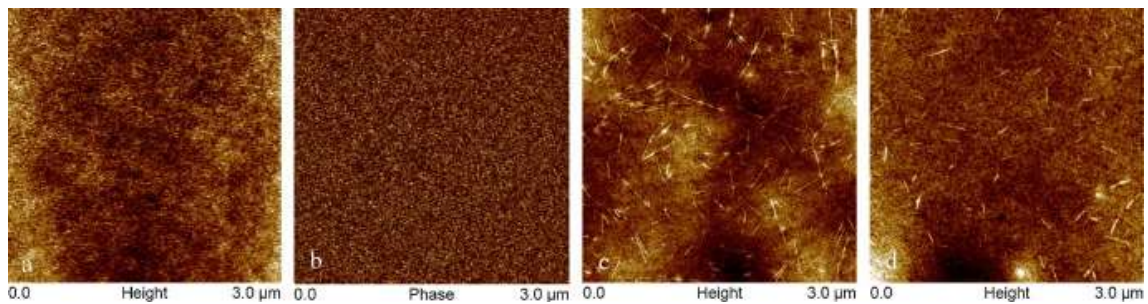


Fig. 9. AFM (a) height and (b) phase images of WBPU, and AFM height images of (c) WBPU-1<sub>son</sub> and (d) WBPU-1<sub>syn</sub> nanocomposites.

Dynamic contact angle ( $\Theta$ ) values of WBPU and nanocomposites containing 1 wt% of CNC, which reveal the hydrophilicity of the films, are shown in Fig. 10. Generally, three main regions can be observed during experiments. The first region corresponds to the advancing contact angle ( $\Theta_a$ ) regime, where  $h$  remains nearly constant while the drop volume and radius are increased. In this region,  $h_a$  is determined by averaging the advancing contact angle values measured in this domain [34]. In addition, usually the advancing contact angle values are quite similar to the values obtained by static contact angle method [35]. In the

region corresponding to the receding contact angle ( $\theta_r$ ), generally lower contact angle values are obtained, and different slopes can be observed derived from the variations in water-surface interactions. The second region is related with the domain just after starting to reduce the volume of the drop, where the base diameter remains unchanged. The third region is related with the simultaneous reduction of the receding contact angle and drop base diameter [36]. Attending to the slope variation in the receding contact angles values curve, due to the second and third region, and considering this transition as  $\theta_r$  [37], it is possible to calculate the equilibrium contact angle ( $\theta_e$ ) based on the equations proposed by Tadmor [37,38]:

$$\theta_e = \arccos((\Gamma_a \cos \theta_a) + (\Gamma_r \cos \theta_r) / (\Gamma_a + \Gamma_r)) \quad (4)$$

$$\Gamma_a = (\sin^3 \theta_a / (2 - 3 \cos \theta_a + \cos^3 \theta_a))^{1/3} \quad (5)$$

$$\Gamma_r = (\sin^3 \theta_r / (2 - 3 \cos \theta_r + \cos^3 \theta_r))^{1/3} \quad (6)$$

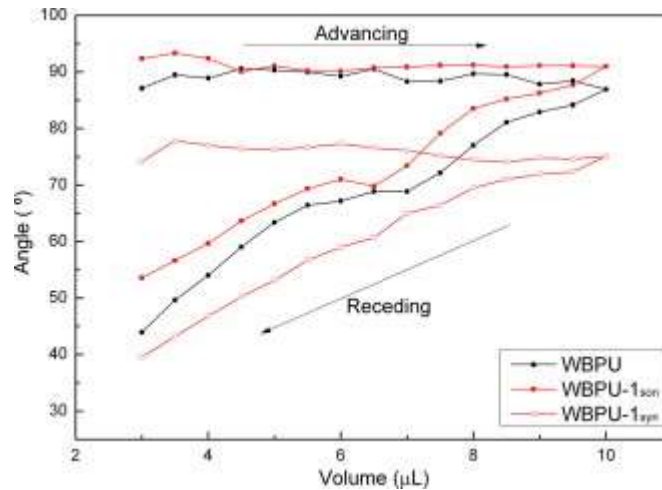


Fig. 10. Advancing and receding water contact angles of films.

Matrix and nanocomposites films show the equilibrium contact angle values of  $82.8^\circ$ ,  $84.8^\circ$  and  $71.0^\circ$  for WBPU, WBPU-1<sub>son</sub> and WBPU-1<sub>syn</sub> respectively, which implies a different hydrophilic behavior of the nanocomposites even though having the same composition. Slightly higher  $\theta_e$  value has been obtained for WBPU-1<sub>son</sub> nanocomposite comparing with WBPU matrix, whereas in the case of WBPU-1<sub>syn</sub>, quite lower  $\theta_e$  value has been observed. It could be due to the arrangement of the CNC in the matrix. As it has been viewed in WBPU-1<sub>son</sub> AFM images, CNC seem to be deposited over the WBPU implying that probably, despite the hydrophilic character, CNC could interfere in the diffusion of water molecules through the film surface considering their high aspect ratio. Otherwise, in WBPU-1<sub>syn</sub> assuming that CNC are partially embedded in the WBPU, and considering the hydrophilic character of CNC, water molecules diffusion could be favored.

In this work, the classical mixing by sonication and the alternative in-situ routes were used to prepare homogeneous WBPU-CNC dispersions first, and thereafter by casting, nanocomposites films containing 1 and 3 wt% of high aspect ratio CNC. The homogeneous dispersion facilitated the suitable casting process promoting WBPU-CNC interactions during the transparent films formation. AFM images showed a homogeneous distribution of CNC in the nanocomposites without the presence of agglomerates. The entire length of dispersed CNC was observed in nanocomposite prepared by casting whereas shorter CNC were observed in nanocomposite prepared in-situ, suggesting that CNC are partially embedded in the matrix due to intercalation among WBPU particles when were added during such particles formation. FTIR results supported this observation. The alternative in-situ route resulted in enhanced WBPU-CNC interactions, which hinder the soft segments chains to arrange in ordered structures, avoiding even completely the crystallization of soft domain in WBPU-3<sub>syn</sub> sample. Thus, WBPU-CNC interactions provided higher E' values than the matrix and an improvement of about 20-30 °C in the thermomechanical stability. TGA results revealed also that WBPU-CNC interactions improve the stabilization of urethane groups delaying the T<sub>m</sub> value about 30 °C comparing with the matrix. Regarding to mechanical properties of the films, it was observed that CNC addition route, as well as content, influenced in the mechanical performance of the films, showing always an effective reinforcing effect. Nanocomposites exhibited different hydrophilic behavior, which would be related with the disposition of CNC in the nanocomposite.

#### *Acknowledgments*

Financial support from the Basque Government (IT-776-13) and from the Spanish Ministry of Economy and Competitiveness (MINECO) (MAT2013-43076-R) is gratefully acknowledged. We also wish to acknowledge the “Macrobehaviour-Mesostructure-Nanotechnology” and “Servicio Central de Análisis de Bizkaia” SGIker units from the University of the Basque Country, for their technical support. A.S.-E. thanks the University of the Basque Country for Ph.D. grant (PIF/UPV/12/201).

#### *References*

- [1] E. Delebecq, J.P. Pascault, B. Boutevin, F. Ganachaud, On the versatility of urethane/urea bonds: reversibility, blocked isocyanate, and non-isocyanate polyurethane, *Chem. Rev.* 113 (2013) 80–118.
- [2] I. Yilgör, E. Yilgör, G.L. Wilkes, Critical parameters in designing segmented polyurethanes and their effect on morphology and properties: a comprehensive review, *Polymer* 58 (2015) A1–A36.
- [3] D.K. Chattopadhyay, K.V.S. Raju, Structural engineering of polyurethane coatings for high performance applications, *Prog. Polym. Sci.* 32 (2007) 352–418.
- [4] R.M.A. Domingues, M.E. Gomes, R.L. Reis, The potential of cellulose nanocrystals in tissue engineering strategies, *Biomacromolecules* 15 (2014) 2327–2346.
- [5] Y. Habibi, L.A. Lucia, O.J. Rojas, Cellulose nanocrystals: chemistry, self-assembly, and applications, *Chem. Rev.* 110 (2010) 3479–3500.
- [6] G. Mondragon, S. Fernandes, A. Retegi, C. Peña, I. Algar, A. Eceiza, et al, A common strategy to extracting cellulose nanoentities from different plants, *Ind. Crops Prod.* 55 (2014) 140–148.
- [7] S.J. Eichhorn, Cellulose nanowhiskers: promising materials for advanced applications, *Soft Matter* 7 (2011) 303–315.

- [8] X.M. Dong, J.F. Revol, D.G. Gray, Effect of microcrystallite preparation conditions on the formation of colloid crystals of cellulose, *Cellulose* 5 (1998) 19–32.
- [9] M.A.S. Azizi Samir, F. Alloin, A. Dufresne, Review of recent research into cellulosic whiskers, their properties and their application in nanocomposite field, *Biomacromolecules* 6 (2005) 612–626.
- [10] M. Mariano, N. El Kissi, A. Dufresne, Cellulose nanocrystals and related nanocomposites: review of some properties and challenges, *J. Polym. Sci., Part B: Polym. Phys.* 52 (2014) 791–806.
- [11] A. Dufresne, Preparation of cellulose nanocomposites, in: *Interface Eng. Nat. Fibre Compos.*, Woodhead Publishing Limited, 2011, pp. 82–116.
- [12] Y. Li, A.J. Ragauskas, Cellulose nano whiskers as a reinforcing filler in polyurethanes, in: *Adv. Divers. Ind. Appl. Nanocomposites*, InTech, 2011, pp. 17–36.
- [13] A. Saralegi, L. Rueda, L. Martin, A. Arbelaiz, A. Eceiza, M.A. Corcuera, From elastomeric to rigid polyurethane/cellulose nanocrystal bionanocomposites, *Compos. Sci. Technol.* 88 (2013) 39–47.
- [14] A. Santamaria-Echart, A. Arbelaiz, A. Saralegi, B. Fernández-d'Arlas, A. Eceiza, M. Corcuera, Relationship between reagents molar ratio and dispersion stability and film properties of waterborne polyurethanes, *Colloid. Surf. A: Physicochem. Eng. Aspects* 482 (2015) 554–561.
- [15] I. Kvien, B.S. Tanem, K. Oksman, Characterization of cellulose whiskers and their nanocomposites by atomic force and electron microscopy, *Biomacromolecules* 6 (2005) 3160–3165.
- [16] T. Abitbol, E. Kloser, D.G. Gray, Estimation of the surface sulfur content of cellulose nanocrystals prepared by sulfuric acid hydrolysis, *Cellulose* 20 (2013) 785–794.
- [17] S. Camarero Espinosa, T. Kuhnt, E.J. Foster, C. Weder, Isolation of thermally stable cellulose nanocrystals by phosphoric acid hydrolysis, *Biomacromolecules* 14 (2013) 1223–1230.
- [18] Z. Gao, J. Peng, T. Zhong, J. Sun, X. Wang, C. Yue, Biocompatible elastomer of waterborne polyurethane based on castor oil and polyethylene glycol with cellulose nanocrystals, *Carbohydr. Polym.* 87 (2012) 2068–2075.
- [19] L. Rueda, A. Saralegi, B. Fernández-d'Arlas, Q. Zhou, A. Alonso-Varona, L.A. Berglund, et al, In situ polymerization and characterization of elastomeric polyurethane–cellulose nanocrystal nanocomposites. Cell response evaluation, *Cellulose* 20 (2013) 1819–1828.
- [20] X. Cao, H. Dong, C.M. Li, New nanocomposite materials reinforced with flax cellulose nanocrystals in waterborne polyurethane, *Biomacromolecules* 8 (2007) 899–904.
- [21] H. Liu, S. Cui, S. Shang, D. Wang, J. Song, Properties of rosin-based waterborne polyurethanes/cellulose nanocrystals composites, *Carbohydr. Polym.* 96 (2013) 510–515.
- [22] C. Fang, X. Zhou, Q. Yu, S. Liu, D. Guo, Synthesis and characterization of low crystalline waterborne polyurethane for potential application in water-based ink binder, *Prog. Org. Coat.* 77 (2014) 61–71.
- [23] D.K. Chattopadhyay, D.C. Webster, Thermal stability and flame retardancy of polyurethanes, *Prog. Polym. Sci.* 34 (2009) 1068–1133.
- [24] F.M.B. Coutinho, M.C. Delpech, T.L. Alves, A.A. Ferreira, Degradation profiles of cast films of polyurethane and poly(urethane-urea) aqueous dispersions based on hydroxy-terminated polybutadiene and different diisocyanates, *Polym. Degrad. Stab.* 81 (2003) 19–27.

- [25] S.M. Cakic, J.V. Stamenkovic, D.M. Djordjevic, I.S. Ristic, Synthesis and degradation profile of cast films of PPG–DMPA–IPDI aqueous polyurethane dispersions based on selective catalysts, *Polym Degrad Stab* 94 (2009) 2015–2022.
- [26] X. Cao, Y. Habibi, L.A. Lucia, One-pot polymerization, surface grafting, and processing of waterborne polyurethane–cellulose nanocrystal nanocomposites, *J. Mater. Chem.* 19 (2009) 7137–7145.
- [27] M. Roman, W.T. Winter, Effect of sulfate groups from sulfuric acid hydrolysis on the thermal degradation behavior of bacterial cellulose, *Biomacromolecules* 5 (2004) 1671–1677.
- [28] N. Wang, E. Ding, R. Cheng, Thermal degradation behaviors of spherical cellulose nanocrystals with sulfate groups, *Polymer* 48 (2007) 3486–3493.
- [29] H. Liu, J. Song, S. Shang, Z. Song, D. Wang, Cellulose nanocrystal/silver nanoparticle composites as bifunctional nanofillers within waterborne polyurethane, *ACS Appl. Mater. Interfaces* 4 (2012) 2413–2419.
- [30] Q. Zhao, G. Sun, K. Yan, A. Zhou, Y. Chen, Novel bio-antifelting agent based on waterborne polyurethane and cellulose nanocrystals, *Carbohydr. Polym.* 91 (2013) 169–174.
- [31] P.S. De Oliveira Patricio, I.M. Patricio, N.C.F. Da Silva, E. Ayres, F.V. Pereira, R.L. Oréfica, Tailoring the morphology and properties of waterborne polyurethanes by the procedure of cellulose nanocrystal incorporation, *Eur. Polym. J.* 49 (2013) 3761–3769.
- [32] L. Rueda, B. Fernández d’Arlas, Q. Zhou, L.A. Berglund, M.A. Corcuera, I. Mondragon, et al, Isocyanate-rich cellulose nanocrystals and their selective insertion in elastomeric polyurethane, *Compos. Sci. Technol.* 71 (2011) 1953–1960.
- [33] Y. Wang, H. Tian, L. Zhang, Role of starch nanocrystals and cellulose whiskers in synergistic reinforcement of waterborne polyurethane, *Carbohydr. Polym.* 80 (2010) 665–671.
- [34] C.N.C. Lam, R. Wu, D. Li, M.L. Hair, A.W. Neumann, Study of the advancing and receding contact angles: liquid sorption as a cause of contact angle hysteresis, *Adv. Colloid Interface Sci.* 96 (2002) 169–191.
- [35] D. Polster, H. Graaf, Advancing and receding angles – dynamic contact angle measurements on mixed alkyl monolayers, *Appl. Surf. Sci.* 265 (2013) 88– 93.
- [36] P.R. Waghmare, S.K. Mitra, Contact angle hysteresis of microbead suspensions, *Langmuir* 26 (2010) 17082–17089.
- [37] W. Zhang, P.R. Waghmare, L. Chen, Z. Xu, S.K. Mitra, Interfacial rheological and wetting properties of deamidated barley proteins, *Food Hydrocoll.* 43 (2015) 400–409.
- [38] R. Tadmor, Line energy and the relation between advancing, receding, and young contact angles, *Langmuir* 20 (2004) 7659–7664.